technologies

MDPI

Article

Comparative Study of Hydrometallurgical and Pyrometallurgical ZnO Recovery from Mixed Metallurgical Sludge

Bruno Kostura [1,*], Radim Škuta [2], Vladislav Kurka [1], Vlastimil Matějka [2], Marek Velička [2], Facundo Barraque [2], Michal Ritz [2], Jana Seidlerová [2], Silvie Vallová [2] and Jozef Vlček [1]

[1] The Material and Metallurgical Research Co., Ltd., Pohraniční 693/31, Vítkovice, 703 00 Ostrava, Czech Republic
[2] Faculty of Materials Science and Technology, VSB–Technical University of Ostrava, 17. listopadu 15, 708 00 Ostrava-Poruba, Czech Republic; vlastimil.matejka@vsb.cz (V.M.); facundo.barraque@vsb.cz (F.B.)
* Correspondence: bruno.kostura@mmvyzkum.cz

Abstract

The recovery of zinc from mixed steelmaking and blast furnace sludge was investigated through a direct comparison of the hydrometallurgical acetic acid leaching process and pyrometallurgical processing using coke dust as a reductive agent, with particular emphasis on the structure and functional properties of the resulting ZnO products. The mixed sludge contained 9.71 wt.% ZnO, with zinc occurring predominantly in the form of stable ferritic phases, mainly franklinite ($(ZnFe^{II})Fe_2O_4$). Hydrometallurgical treatment using 1 mol·dm^{-3} acetic acid resulted in only a limited relative decrease in Zn content (16.8%) based on solid-phase concentrations, as mainly readily soluble zinc phases were dissolved, while ferrite-bound zinc remained largely unaffected. In contrast, pyrometallurgical treatment of the sludge–coke dust mixture at 1200 °C enabled highly effective zinc volatilization, reducing the residual Zn content below 0.05 wt.% and resulting in a relative decrease in Zn content of 99.5% based on solid-phase concentrations. Characterization by XRD, FTIR, SEM, and EDS revealed substantial differences between the products obtained by the two processing routes. The pyrometallurgically prepared ZnO-rich product exhibited higher crystallinity, well-developed rod-like morphology, and substantially lower Fe and Pb contamination than the hydrometallurgically prepared material. In contrast, the hydrometallurgical product showed lower crystallinity and elevated Fe and Pb contents and therefore represented a highly contaminated ZnO-rich oxide mixture. Photocatalytic tests using Rhodamine B showed measurable but low activity of the pyrometallurgical product, with approximately 18% degradation after 120 min of UV irradiation, whereas the hydrometallurgical product was practically inactive. Overall, carbothermic treatment provided substantially more effective Zn removal than acetic acid leaching, although the recovered ZnO-rich product exhibited only limited photocatalytic activity.

Keywords: metallurgical sludge; waste recycling; hydrometallurgy; pyrometallurgy; zinc oxide; circular economy

Check for updates

Academic Editor: Miklas Scholz

Received: 23 July 2026
Revised: 4 September 2026
Accepted: 5 September 2026
Published: 8 September 2026

Copyright: © 2026 by the authors. Licensee MDPI, Basel, Switzerland. This article is an open access article distributed under the terms and conditions of the Creative Commons Attribution (CC BY) license.

1. Introduction

The iron and steel industry ranks among the most resource- and energy-intensive industrial sectors and is simultaneously a major generator of solid by-products and process residues. These materials—primarily dusts, sludges, and aqueous suspensions—originate from off-gas cleaning systems and process water treatment units [1,2]. They are typically enriched in iron oxides, calcium-bearing phases, and residual carbon, which makes

them potentially valuable secondary raw materials within the context of circular economy strategies [3]. However, their direct reuse is often impeded by elevated concentrations of volatile and toxic elements, particularly zinc, lead, and cadmium. These contaminants not only complicate their reintegration into metallurgical processes but also pose significant long-term environmental risks when landfilled [4]. In addition, legacy deposits of metallurgical sludges and tailings represent a persistent environmental burden, reinforcing the need for their efficient valorization in line with current Best Available Techniques (BAT) requirements [5].

Zinc is among the most problematic contaminants in iron and steelmaking operations. Under high-temperature conditions, it is readily reduced and volatilized, subsequently condensing in cooler sections of processing units and gas-cleaning systems, where it accumulates as fine particulate matter [6]. This internal zinc cycling contributes to increased dust generation, process instability, and accelerated wear of refractory linings [7,8]. Consequently, stringent limits are imposed on the zinc content of feed materials used in ironmaking and steelmaking processes [9]. The effectiveness of zinc removal from metallurgical residues is strongly governed by its mineralogical association. Zinc present as oxide or in weakly bound carbonate and hydroxide phases is relatively amenable to dissolution. In contrast, zinc incorporated into chemically stable ferritic spinel structures—particularly franklinite ($ZnFe_2O_4$)—exhibits high resistance to conventional leaching agents [10,11].

In recent years, hydrometallurgical routes have been extensively investigated for selective zinc extraction from steelmaking residues, either as a pretreatment prior to pyrometallurgical processing or as a standalone recycling pathway for suitable material streams [12]. Within this framework, organic acids have attracted increasing attention due to their potential for enhanced selectivity towards zinc while suppressing iron dissolution [13,14]. For example, acetic acid (CH_3COOH) has been shown to selectively leach zincite from steelmaking sludges under mild conditions, preferentially dissolving ZnO while leaving more stable iron-bearing phases largely unaffected [15]. Similarly, butyric acid has been reported to achieve approximately 50% zinc removal under optimized conditions with minimal iron co-dissolution [16]. Acrylic acid (C_2H_3COOH) has also been investigated, with zinc dissolution attributed primarily to Lewis's acid–base interactions, while iron solubility is strongly controlled by solution pH [17]. In contrast, sulfuric acid remains one of the most widely used leaching agents due to its high efficiency. Its performance can be further enhanced through process intensification techniques, such as ultrasound-assisted leaching, which accelerates reaction kinetics and improves zinc recovery from ZnO-rich materials [18]. Moreover, hybrid leaching systems combining organic acids (e.g., malic acid) with sulfuric acid have been developed to produce high-purity ZnO [19]. Beyond conventional aqueous systems, growing attention is being directed towards alternative and more environmentally benign solvents, including deep eutectic solvents (DESs) based on choline chloride and urea. These systems, particularly when combined with suitable complexing agents, have demonstrated promising selectivity for zinc-bearing phases while limiting the co-dissolution of unwanted components [20]. The choice of lixiviant remains a key factor in zinc recovery from metallurgical wastes, as organic acids generally provide improved selectivity towards zinc-bearing phases, whereas mineral acids are more effective in dissolving stable zinc-containing compounds and achieving higher overall extraction efficiencies [21].

Pyrometallurgical approaches to zinc recovery exploit the high vapor pressure of zinc at elevated temperatures, typically in the range of 900–1200 °C. Under reducing conditions, zinc-bearing phases are converted to metallic zinc, which volatilizes and is subsequently transported by process gases to cooler zones. There, controlled reoxidation and condensation lead to the formation of fine-grained ZnO, which is captured in gas-cleaning

systems [22]. The Waelz process, based on rotary kiln operation with a carbonaceous reductant, remains the industrial benchmark for the treatment of zinc-bearing dusts and sludges. However, it is associated with several limitations, including high energy demand, significant carbon consumption, and a correspondingly high carbon footprint [23]. Additional drawbacks include the generation of secondary slags, limited tolerance to feed variability, and challenges associated with internal zinc circulation in integrated steel plants [24].

Alongside process optimization, increasing emphasis is placed on the quality and applicability of recovered products. Iron-rich residues with sufficiently low zinc content can be recycled back into ironmaking and steelmaking processes or utilized as secondary raw materials following suitable agglomeration [8,25]. Similarly, zinc oxide recovered from metallurgical off gases represents a valuable secondary product, particularly for non-critical applications such as rubber compounding, where ZnO serves as a vulcanization activator [26,27].

This study aims to provide a systematic comparison of ZnO products obtained both via the hydrometallurgical leaching process, using acetic acid solution, and via pyrometallurgical processing using coke dust as a reductive agent of mixed metallurgical sludges. In contrast to most previous studies, which typically focus on well-defined model materials, the present work addresses complex, heterogeneous residues originating from both blast furnace and steelmaking operations. Furthermore, the investigated sludge is landfilled without further utilization, representing both an environmental burden and a loss of potentially valuable secondary resources. Accordingly, the proposed approach links waste remediation with recovery and the valorization of accumulated metallurgical wastes.

The novelty of this study lies not only in the direct comparison of fundamentally different processing approaches under comparable conditions, but also in the integrated evaluation of both process performance and product quality. Emphasis is placed on the physicochemical characterization of the resulting ZnO, enabling a more application-oriented assessment than is commonly reported in the literature.

The specific objectives of this work are:

(I) To evaluate and compare the efficiency of zinc removal by selected hydrometallurgical and pyrometallurgical routes and to comprehensively characterize the resulting ZnO products;

(II) To assess the suitability of the recovered ZnO for subsequent utilization, with particular regard to circular economy principles and potential industrial applications.

2. Materials and Methods

Mixed metallurgical sludge originating from the Ostrava industrial agglomeration was used in this study (GPS 49.673592, 18.655798). The material consisted of steelmaking and blast furnace sludges collected from gas-cleaning systems. Prior to further processing, the sludge was dried at 110 °C overnight, ground in a BRIO BVM laboratory vibration mill, and sieved to a particle size below 0.1 mm to ensure sample homogeneity.

Hydrometallurgical treatment was carried out by acidic leaching. In a typical experiment, 100 g of sludge was contacted with 200 cm^3 of 1 $mol \cdot dm^{-3}$ acetic acid and agitated at 180 rpm for 24 h using a horizontal shaker (IKA HS 260, IKA, Breisgau, Germany) under ambient conditions. These parameters were set according to our previous work in this field [28]. Leaching time of 24 h appeared as optimal. Following leaching, the suspension was filtered, and the solid residue was thoroughly washed with deionized water and dried. Zinc was obtained from the acetate leachate in the form of ZnO by precipitation using 26% aqueous ammonia, while the pH was maintained at 8.5, followed by calcination (200 °C, 2 h).

Pyrometallurgical treatment of sludge was carried out in a rotary kiln with indirect heating of the charge, operated by MMV Co., Ostrava, Czech Republic. The weight of the charge was 100 g and consisted of a mixture of 50 wt.% sludge and 50 wt.% coke oven dust. After homogenization, the charge was placed in a refractory cartridge of the rotary kiln and heated at a rate of 10 °C min^{-1} to a target temperature of 1200 °C in an air atmosphere with a constant flow rate of 100 cm^3 min^{-1}. After reaching 1200 °C, the charge was maintained at this temperature for 60 min to allow carbothermic reduction and Zn volatilization to proceed.

The concentrations of Cd, Cr, Fe, Pb, and Zn in the acetate leachates were determined by inductively coupled plasma atomic emission spectrometry (ICP-AES) using a SPECTRO ARCOS spectrometer (Spectro, Kleve, Germany) equipped with an argon plasma source. Elemental concentrations were determined in accordance with Method 6010D (US EPA, 2014) using calibration curves prepared from single-element stock solutions with a nominal concentration of 1000 ± 50 mg·L^{-1} (Merck, Darmstadt, Germany).

Fourier-transform infrared (FTIR) spectra of sludge samples before and after leaching were recorded using a Thermo Scientific Nicolet iS50 spectrometer equipped with a DTGS detector (Thermo Scientific, Waltham, MA, USA) over the range of 4000–400 cm^{-1}, employing KBr pellet preparation.

Phase composition was determined by X-ray diffraction (XRD) using a MiniFlex 600 (Rigaku, Tokyo, Japan) diffractometer with Co Kα radiation. Diffractograms were collected over a 2θ range of 10–90° and evaluated using the PDF-2 database. The chemical composition of the sludge and coke dust was determined by wavelength-dispersive X-ray fluorescence (WD-XRF) spectroscopy using a SuperMini200 (Rigaku, Tokyo, Japan) spectrometer.

The morphology and microstructure of the samples were examined using a TM4000Plus scanning electron microscope (SEM) (Hitachi Ltd., Tokyo, Japan) equipped with a tungsten filament and an energy-dispersive X-ray spectroscopy (EDS) detector. Prior to analysis, the samples were mounted on 12 mm metallic stubs using conductive carbon tape and sputter-coated with a 5 nm platinum layer using an EM ACE200 sputter coater (Leica Microsystems GmbH, Wetzlar, Germany) under vacuum in an argon atmosphere.

The photocatalytic activity of ZnO samples prepared via hydrometallurgical and pyrometallurgical routes was evaluated through the degradation of Rhodamine B (RhB) in aqueous solution. For each experiment, 150 cm^3 of RhB solution with an initial concentration of 5 mg·dm^{-3} was mixed with 45 mg of powdered ZnO. The suspension was magnetically stirred at 300 rpm in the dark for 1 h to establish adsorption–desorption equilibrium prior to irradiation. Subsequently, the suspension was irradiated in a photocatalytic reactor equipped with a UV LED lamp emitting radiation at a wavelength of 360 nm with an intensity of 7.1 mW·cm^{-2}. During irradiation, 2 cm^3 aliquots were withdrawn after 20, 40, 60, 90, and 120 min using a syringe fitted with a 0.45 μm membrane filter to remove suspended particles.

The absorbance of the filtrates was measured using a Helios ε UV–Vis spectrophotometer (Thermo Electron Corporation—SPECTRONIC, Madison, WI, USA) with 1 cm quartz cuvettes at the maximum absorption wavelength of RhB (552 nm). The photocatalytic activity was expressed as the ratio of residual dye absorbance to the initial absorbance (A/A_0).

3. Characterization of the Mixed Steel and Blast Furnace Sludge

The grain size of the sample was adjusted to below 0.1 mm by grinding and sieving. Elemental analysis was performed by X-ray spectrometry. Carbon and sulfur contents were determined by high-temperature combustion in an oxygen atmosphere followed by IR

detection of the evolved CO_2 and SO_2 gases. The content of the elements was determined using XRFS and expressed in the form of oxides. The resulting chemical composition of the mixed sludge is shown in Table 1.

Table 1. Chemical composition of the mixed sludge (wt.%).

S	C	Fe_{metal}	FeO	Fe_2O_3	Al_2O_3	CaO	SiO_2
0.11	2.2	0.15	13.13	63.77	0.41	1.44	2.13
ZnO	**PbO**	**MnO**	**MgO**	**Cr_2O_3**	**K_2O**	**P_2O_5**	**Na_2O**
9.71	0.42	0.98	0.72	0.25	0.17	0.42	0.40

The X-ray diffraction pattern of the original mixed sludge is shown in Figure 1. The diffraction pattern is dominated by reflections characteristic of spinel-type iron oxides, with magnetite (Fe_3O_4) representing the major crystalline phase. Hematite (Fe_2O_3) was also identified as a secondary iron-bearing phase. Reflections potentially attributable to ZnO are also present. A weaker contribution from quartz or other SiO_2-containing phases cannot be excluded, although the reflection observed at approximately $2\theta = 31^\circ$ cannot be unequivocally assigned to quartz. Overall, the XRD results indicate that the original sludge consists predominantly of Fe-oxide phases, accompanied by zinc-bearing and minor silicate phases.

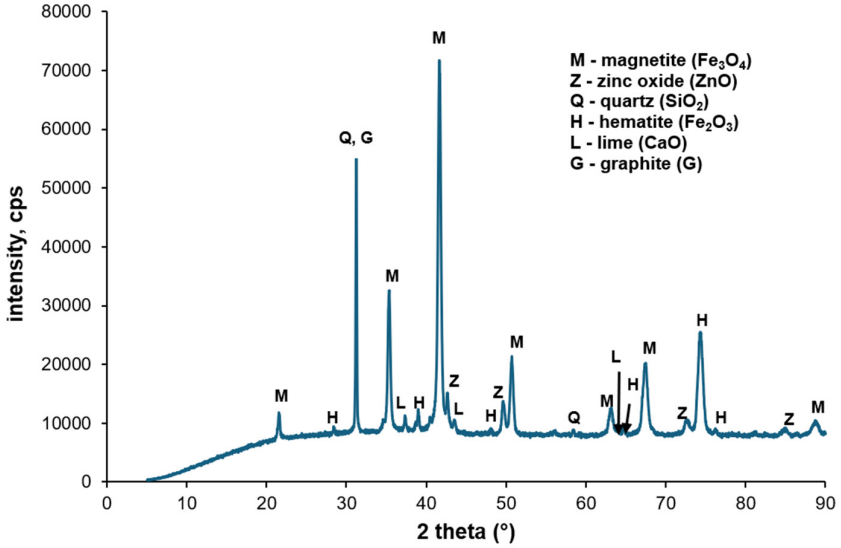


Figure 1. X-ray diffraction pattern of the original sludge.

The quantitative phase analysis presented in Figure 2 indicates that only a minor fraction of zinc is present as zincite (ZnO), whereas the majority of Zn is incorporated in the franklinite spinel phase [$(Zn,Fe^{II})Fe_2O_4$]. This distribution is particularly important with respect to the subsequent zinc recovery, since zinc bound in the chemically stable spinel structure is generally less susceptible to conventional hydrometallurgical leaching than free ZnO. Although no Zn-containing metallic or alloy phases were identified by XRD, the presence of minor amounts of zinc in such forms cannot be completely excluded, particularly if their concentrations are below the detection limit of the method. The quantitative analysis also reveals a relatively high proportion of amorphous material in the sludge, accounting for approximately 42% of the sample.

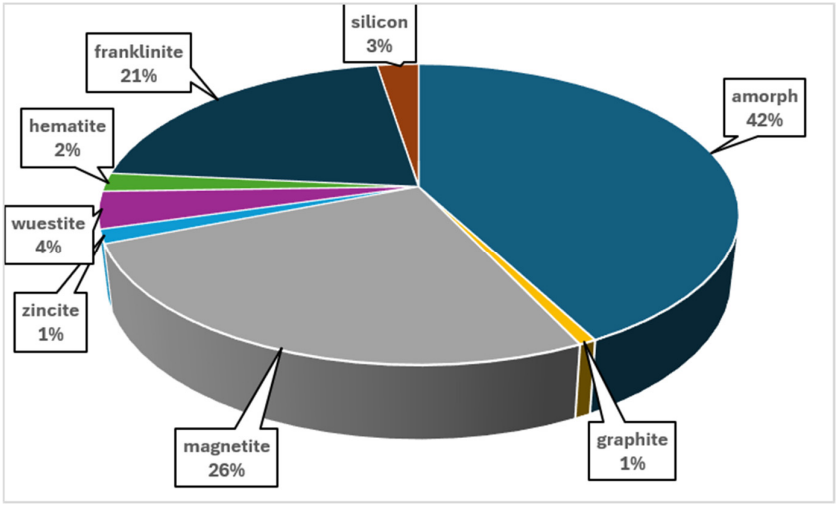


Figure 2. Phase analysis of the mixed sludge.

Figure 3 shows the SEM micrograph of the original mixed metallurgical sludge. The sample exhibits a highly heterogeneous morphology characterized by irregularly shaped metallic particles with a wide particle size distribution. Relatively large particles are extensively covered by fine particulate matter, forming compact agglomerated structures. In addition to these agglomerates, numerous fine particles are also observed separately dispersed throughout the sample. The observed morphology indicates the complex multiphase nature of the mixed sludge and suggests interparticle interactions between coarse and fine fractions.

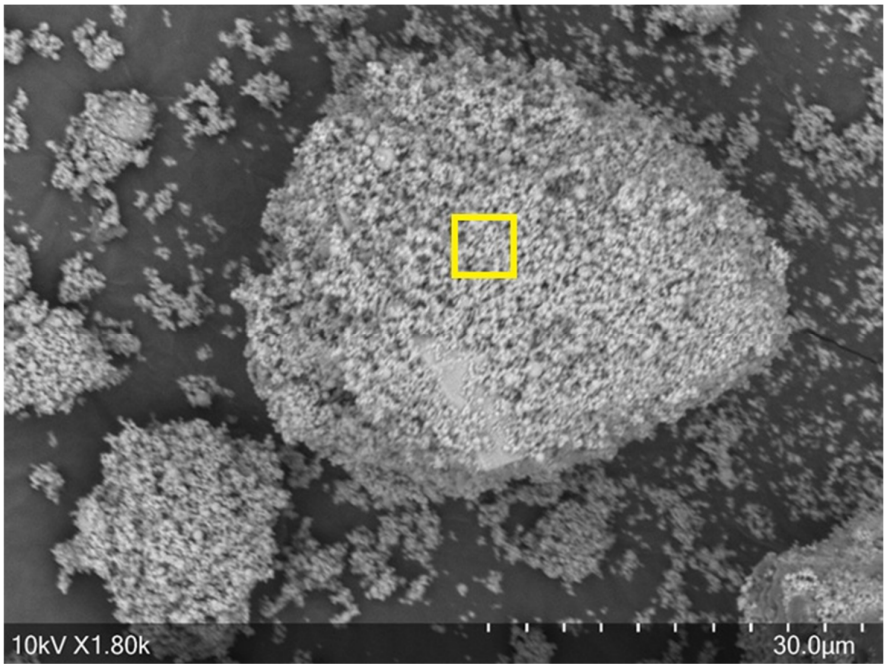


Figure 3. SEM micrograph of the original mixed sludge sample.

4. Hydrometallurgical Separation of Zn as ZnO

Selective zinc leaching is a chemical prerequisite for the zero-waste recycling of steelmaking dust. Zinc spinel ($ZnFe_2O_4$) is the primary barrier to recycling; its decomposition enables the separation of Zn and Fe, allowing them to be returned to production and creating a truly closed material cycle. Most recent studies on this topic show that organic acids (e.g., tartaric acid) can selectively destabilize Zn-rich spinel surface layers, leading to

the selective release of Zn with minimal dissolution of Fe [29]. Thermodynamic modeling confirms that the use of reducing agents (hydrazine, CaO) fundamentally alters the solubility of $ZnFe_2O_4$, even at relatively low temperatures [30,31]. The process thus becomes suitable for low-carbon, closed-loop zinc recycling from EAF dust, with minimal waste generation and reagent recovery.

Hydrometallurgical treatment of mixed metallurgical sludge was carried out using acetic acid. The choice of acetic acid represents a compromise between zinc selectivity, environmental compatibility and operational requirements of the process. To evaluate leaching selectivity and process efficiency, experiments were conducted using two acetic acid concentrations (1 and 2 mol·dm^{-3}) and two solid–liquid ratios, corresponding to 100 and 50 g of sludge per 200 cm^3 of leaching solution.

As summarized in Table 2, the combination of a 1 mol·dm^{-3} acetic acid solution with a solid–liquid ratio of 1:2 (sample 1Ac-100 g) exhibited the most favorable balance between zinc dissolution and leaching selectivity. The table further shows that, in addition to part of the zinc, mainly calcium and a smaller part of oxide-bound iron pass into the leachate.

Table 2. Metal contents in acid leachate.

Sample	Zn (mg·dm^{-3})	Fe (mg·dm^{-3})	Pb (mg·dm^{-3})	Mn (mg·dm^{-3})	Mg (mg·dm^{-3})	Ca (mg·dm^{-3})
1Ac-100 g	11,050	852	684	158	598	4170
1Ac-50 g	5240	916	492	98.8	364	2300
2Ac-100 g	10,300	2090	1110	220	787	4940
2Ac-50 g	5150	1190	563	105	378	2370

Analysis of the solid residue after leaching (Table 3) revealed only a slight decrease in zinc content, indicating that acetic acid preferentially dissolves the more readily soluble Zn-bearing phases, while zinc bound in the stable franklinite structure remains largely unaffected.

Table 3. Chemical composition of the mixed sludge after leaching (wt.%).

S	C	Fe_{metal}	FeO	Fe_2O_3	Al_2O_3	CaO	SiO_2
0.06	2.85	0.15	14.36	67.00	0.36	0.65	1.95
ZnO	**PbO**	**MnO**	**MgO**	**Cr_2O_3**	**K_2O**	**P_2O_5**	**Na_2O**
8.08	0.46	0.96	0.68	0.29	0.12	0.41	0.21

This is also reflected in the comparison of the FTIR spectra of the original and leached mixed sludge shown in Figure 4, where a general decrease in the intensity of several absorption bands is observed after leaching. The bands in the region of approximately 100–700 cm^{-1} are associated mainly with lattice vibrations of metal oxides, particularly iron oxides, whereas the band around 1000 cm^{-1} can be assigned to Si–O vibrations in silicate phases. The bands around 1450 cm^{-1} and 1650 cm^{-1}, attributed to carbonate species and deformation vibrations of H–O–H associated with adsorbed water, respectively, disappear or substantially decrease after leaching. The disappearance of the carbonate-related band indicates dissolution of carbonate-containing phases during acetic acid treatment. However, since no crystalline Zn-containing carbonate phase was clearly identified by XRD, this FTIR feature cannot be specifically assigned to zinc carbonate, and the chemical nature of the dissolved carbonate-bearing phase remains uncertain.

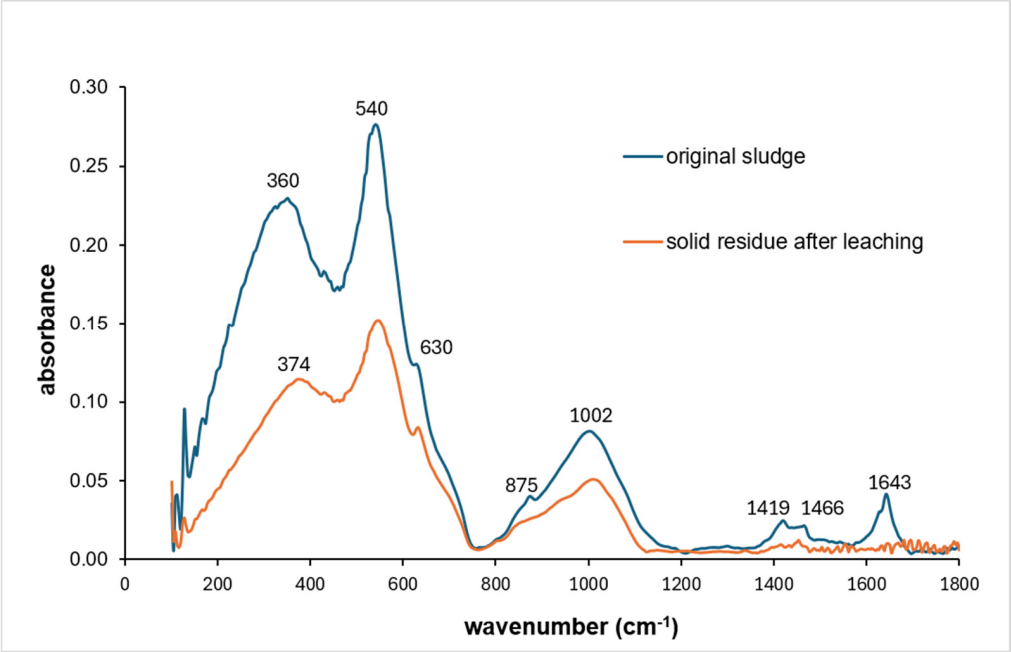


Figure 4. Comparison of FTIR spectra of original and mixed sludge.

Based on the ZnO concentrations in the original sludge (9.71 wt.%) and the solid residue after leaching (8.08 wt.%), the relative decrease in the solid-phase ZnO content was 16.8%, calculated as [(9.71–8.08)/9.71]·100. This value represents a concentration-based estimate rather than a rigorous Zn separation efficiency, because changes in the total solid mass during leaching were not included in the calculation. The reason can be attributed to the relatively high proportion of franklinite ($ZnFe_2O_4$—Figure 2) in the leached sludge. This phase possesses a highly stable spinel structure, characterized by a strongly negative Gibbs free energy of formation ($\Delta G < 0$). Acetic acid, selected for its high selectivity towards zinc, is not strong enough ($pK_a = 4.76$) to protonate O^{2-}, disrupt the Fe–O framework, and release Zn^{2+} and Fe^{3+} into solution. Low H^+ ion activity in the solution causes the Gibbs energy of the reaction:

$$ZnFe_2O_4 + 8H^+ \rightarrow Zn^{2+} + 2Fe^{3+} + 4H_2O \quad (1)$$

to be positive and the reaction equilibrium is shifted completely to the left [32]. Zinc bound in the stable ferritic phases remains largely intact and the solid residue after acetic acid leaching cannot therefore be used as a secondary raw material in metallurgy due to the still high zinc content.

5. Pyrometallurgical Separation of Zn as ZnO

For this purpose, a mixture of sludge and coke dust was prepared in a weight ratio of 1:1. The mixture was ground and homogenized, and its grain size was adjusted to below 0.1 mm by sieving. Coke dust was used as a reducing agent due to its high carbon content, as shown in Table 4.

Table 4. Chemical composition of coke dust sample (wt.%).

C	S	Fe_{metal}	FeO	Fe_2O_3	Al_2O_3	CaO	SiO_2	MgO
86.00	0.48	0.14	0.55	0.40	3.47	0.55	6.35	0.23

The efficiency of the pyrometallurgical process was tested for different calcination temperatures of 1000, 1100 and 1200 °C. The results are summarized in Figure 5. It is clear from the figure that the optimal efficiency of the calcination process was achieved at a temperature of 1200 °C, when the zinc content dropped below 0.05%, as shown in Table 5.

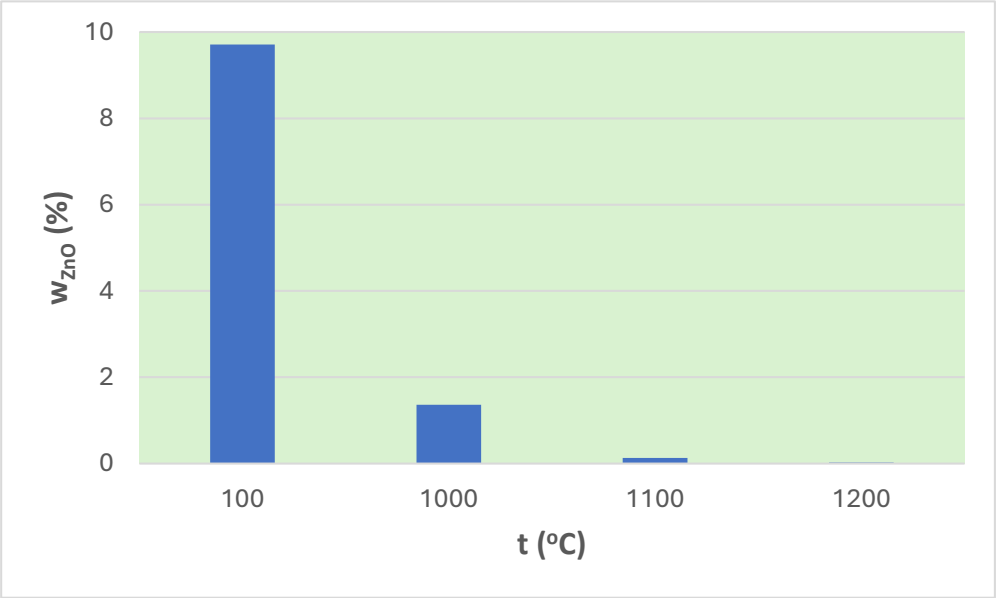


Figure 5. Contents of Zn as ZnO in the calcination residue after calcination at different temperatures.

Table 5. Chemical composition of the solid residue after pyrometallurgical treatment (wt.%).

S	C	Fe_{metal}	FeO	Fe_2O_3	Al_2O_3	CaO	SiO_2
0.42	40.50	33.04	0.25	7.55	1.78	0.95	3.74
ZnO	**PbO**	**MnO**	**MgO**	**Cr_2O_3**	**K_2O**	**P_2O_5**	**Na_2O**
0.02	0.01	0.39	0.45	0.16	0.12	0.20	0.03

During carbothermic treatment, both zincite and zinc ferrite can be reduced by carbon according to Equations (2) and (3):

$$ZnO(s) + C(s) \rightarrow Zn(g) + CO(g) \quad (2)$$

$$ZnFe_2O_4(s) + 4C(s) \rightarrow Zn(g) + 2Fe(s) + 4CO(g) \quad (3)$$

At the treatment temperatures applied, the reduced zinc is volatilized due to its high vapor pressure. After leaving the reducing zone and entering the cooler part of the system, gaseous Zn is re-oxidized by oxygen present in the gas phase, forming ZnO particles (Equation (4)):

$$2Zn(g) + O_2(g) \rightarrow 2ZnO(s) \quad (4)$$

Thus, the carbothermic treatment simultaneously promotes zinc removal from both ZnO and $ZnFe_2O_4$, while iron originating from zinc ferrite remains predominantly in the solid residue in a reduced metallic form.

This is confirmed by the comparison of the X-ray diffraction records of the mixture before and after pyrometallurgical treatment in Figure 6.

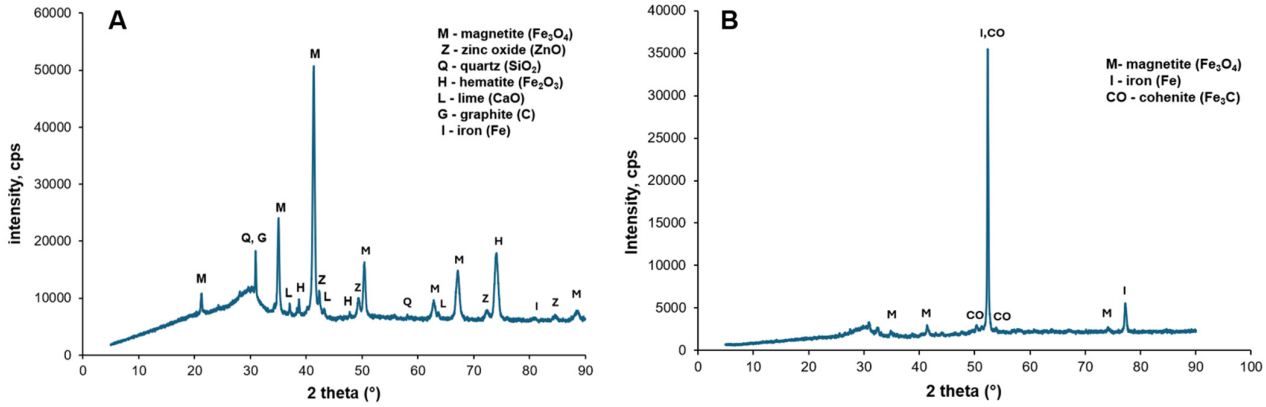


Figure 6. Comparison of X-ray diffraction patterns of the sludge and coke dust mixture before (**A**) and after (**B**) pyrometallurgical processing.

The following important changes were observed in the X-ray diffraction pattern after pyrometallurgical treatment. The ZnO diffraction lines completely disappeared. Furthermore, part of the magnetite was transformed into metallic iron. The broad diffusion band observed in the 2θ range of approximately 20–30° is characteristic of a poorly ordered or amorphous carbonaceous material [33]. The intensity of the diffraction line with a maximum at around 31° 2Theta is reduced in the calcined sample, which can be attributed to the decomposition of calcite that was present in the coke dust. The fact that it did not completely disappear shows that graphite and SiO_2 are still present in the calcined sample, which agrees with the results of the elemental analysis. The relative decrease in Zn content in the pyrometallurgically processed sludge sample, calculated based on solid-phase concentrations, was 99.5%. At the same time, an Fe concentrate with a very low Zn content was obtained, which can be reused in the production of iron and steel.

6. Characterization of ZnO Obtained Hydrometallurgically and Pyrometallurgically

A visual comparison of products prepared by hydrometallurgical and pyrometallurgical separation from mixed metallurgical sludge is shown in Figure 7. While the pyrometallurgically obtained ZnO (Figure 7B) exhibits the typical white appearance of ZnO, the hydrometallurgically prepared sample (Figure 7A) shows a distinct reddish-brown coloration. Although the white appearance of the pyrometallurgical product is consistent with ZnO containing relatively low levels of colored impurities, color alone cannot be considered a direct indicator of chemical purity.

The reddish-brown coloration of the hydrometallurgically recovered ZnO can primarily be attributed to the co-precipitation of dissolved iron species during ammoniacal precipitation and their subsequent transformation into iron oxide phases, particularly α-Fe_2O_3, during calcination. The intense coloration of hematite may significantly affect the appearance of ZnO even at relatively low concentrations. Minor contributions from Zn–Fe mixed oxides, including $ZnFe_2O_4$, and other co-precipitated impurities cannot be excluded, which is consistent with the analytical data of the acid leachate (Table 2). The hydrometallurgically prepared sample therefore represents a complex, highly contaminated mixture of oxides with a majority of ZnO.

The structural character of the two materials differs significantly, which is related to the different mechanisms of their formation. Hydrometallurgically prepared ZnO is formed by precipitation from solutions, which usually leads to the formation of finely dispersed, low-crystalline or partially amorphous particles. In contrast, pyrometallurgical ZnO is formed by nucleation and growth from the gas phase (oxidation of Zn vapor), which

promotes the formation of well-developed crystals with a higher degree of structural order. These differences are clearly confirmed by X-ray diffraction analysis (Figure 8).

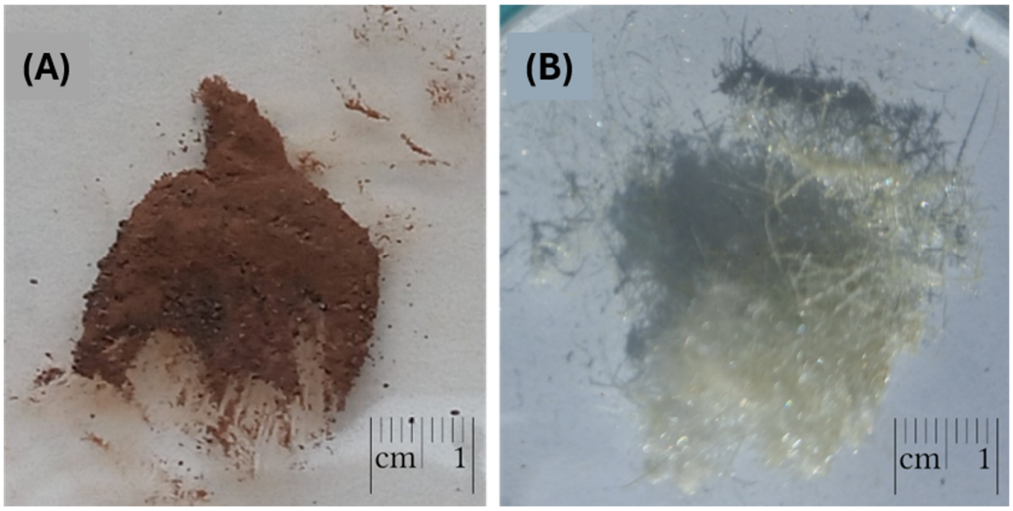


Figure 7. Visual comparison of ZnO-based products separated hydrometallurgically (**A**) and pyrometallurgically (**B**).

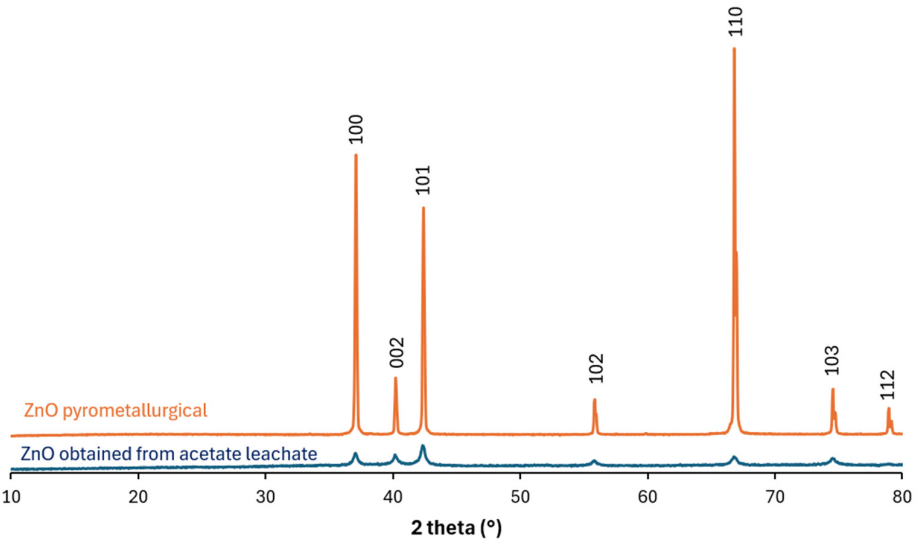


Figure 8. Comparison of X-ray diffraction patterns of ZnO-based products obtained hydrometallurgically and pyrometallurgically.

The diffraction pattern of the pyrometallurgically prepared sample shows sharp and intense reflections corresponding to the hexagonal wurtzite structure of ZnO, which is indicative of high crystallinity and low density of structural defects. In contrast, the hydrometallurgically prepared sample is characterized by broader and significantly less intense diffraction peaks, which indicates lower crystallinity, smaller crystallite size and potentially a higher proportion of defective or amorphous regions. The increased peak width can also be associated with micro-deformations of the crystal lattice and the presence of substitutional or interstitial impurities, which is again in accordance with Table 3.

SEM analysis (Figure 9) further confirms the fundamental differences in particle morphology. Pyrometallurgically prepared ZnO (Figure 9B) is formed by well-defined rod-like to needle-like crystals, which corresponds to the anisotropic growth of ZnO crystals along the preferred crystallographic directions (typically the c-axis). This type of morphology is often associated with higher crystallinity and lower defect concentration.

The hydrometallurgically prepared sample (Figure 9A) on the other hand shows aggregates of irregular, sharp-edged particles with a broad range of sizes and low morphological uniformity. Such a structure may lead to a reduced specific surface area and limited availability of active surface centers.

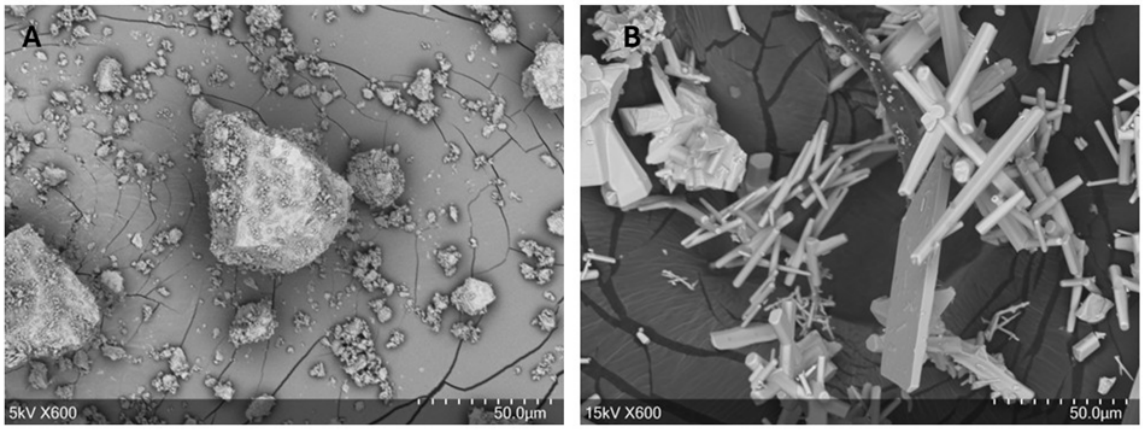


Figure 9. Comparison of SEM images of ZnO-based products obtained hydrometallurgically (**A**) and pyrometallurgically (**B**).

The chemical composition of the ZnO products obtained by hydrometallurgical and pyrometallurgical processing is summarized in Table 6. Significant differences in chemical purity were observed between the two separation routes. The ZnO produced by the pyrometallurgical method exhibited a markedly higher Zn content (75.8 wt.%) compared with the hydrometallurgically prepared sample (39.1 wt.%). Simultaneously, the pyrometallurgical product contained only trace concentrations of Fe (0.1 wt.%) and no detectable Pb, indicating highly effective separation of undesirable metallic impurities during the reduction–volatilization process.

Table 6. Chemical composition ZnO samples produced by hydrometallurgical and pyrometallurgical methods.

	Hydrometallurgical Method	**Pyrometallurgical Method**
Element	**wt.%**	**wt.%**
O	22.0	20.1
Na	8.3	3.7
Al	1.9	0.2
Si	2.7	0.1
Fe	13.3	0.1
Zn	39.1	75.8
Pb	12.7	0

During the pyrometallurgical treatment of steelmaking sludge with coke dust at 1200 °C, zinc is readily reduced and volatilized due to its low boiling point (907 °C) and high vapor pressure. In contrast, although lead is also potentially volatile, its transfer to the gas phase may be limited by several chemical and physical mechanisms [34,35]. The sludge contains significant amounts of gangue, particularly silicon dioxide (SiO_2), calcium oxide (CaO), and iron oxides. PbO can react with SiO_2 present in the gangue to form thermodynamically stable lead silicates, thereby suppressing its reduction and volatilization. In addition, the simultaneous carbothermic reduction of iron oxides produces

metallic Fe, within which reduced Pb may become physically entrapped or associated with Fe-rich phases. At a temperature of 1200 °C, intensive sintering of fine dust particles and iron is likely to occur. This sintering can lead to the encapsulation of liquid lead (melting point 327 °C) in an iron-rich matrix. Unlike Zn, which rapidly volatilizes under these conditions, Pb remains liquid because of its considerably higher boiling point (1749 °C), and its diffusion through the sintered material is therefore limited. These mechanisms may explain the preferential volatilization of Zn and the retention of a substantial fraction of Pb in the solid residue.

In contrast, the ZnO sample obtained via the hydrometallurgical route showed substantially elevated concentrations of Fe (13.3 wt.%) and Pb (12.7 wt.%). These results suggest that, during acid leaching, part of the accompanying metal-bearing phases was dissolved together with zinc and subsequently incorporated into the precipitated product. The higher contents of Al and Si in the hydrometallurgical ZnO further confirm the lower selectivity of this separation approach.

Overall, the EDS analysis demonstrates that the pyrometallurgical treatment yielded a significantly purer ZnO-rich product with considerably lower contamination by accompanying elements.

The photocatalytic activities of ZnO samples prepared by hydrometallurgical and pyrometallurgical processes (Figure 10) show that the pyrometallurgically prepared ZnO exhibits some photocatalytic activity, while the hydrometallurgical sample is practically inactive. The baseline control curve (sample without ZnO) increases above 1.000 after 120 min. of irradiation. This phenomenon can be attributed to gradual heating of the liquid sample and therefrom resulting solvent evaporation.

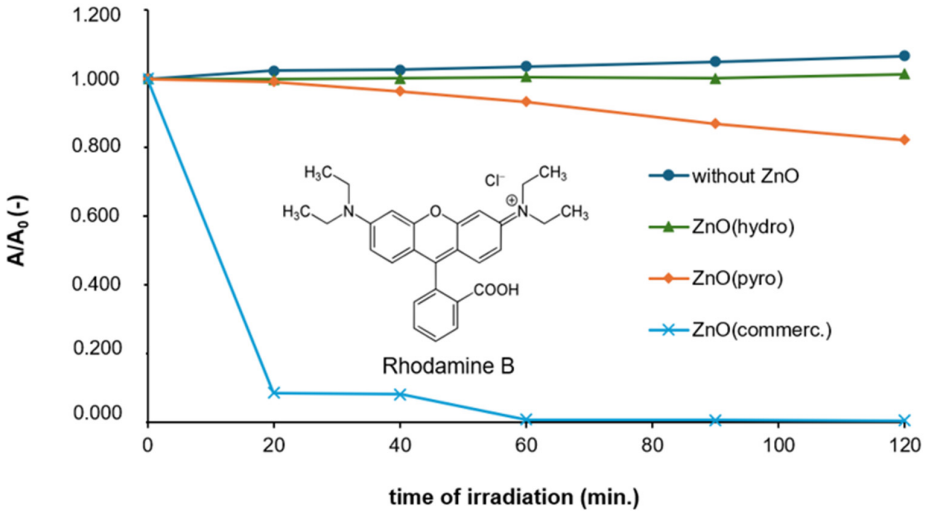


Figure 10. Time course of degradation of Rhodamine B using ZnO obtained by hydrometallurgical and pyrometallurgical processes.

The almost zero photocatalytic activity of the hydrometallurgically produced ZnO is most likely associated with its coarser particle morphology and consequently lower specific surface area (SSA), resulting in a reduced number of accessible active sites. The specific surface areas (SSA) of the ZnO samples were not measured in this study; therefore, their possible influence on photocatalytic activity can only be discussed based on literature data for comparable materials. Hydrometallurgically prepared ZnO typically exhibits SSA values of approximately 10–25 $m^2\ g^{-1}$ [36], whereas pyrometallurgically produced ZnO generally shows even lower values (1–15 $m^2\ g^{-1}$) [37]. These values are considerably below those reported for commercial nanostructured ZnO (up to approximately 60 $m^2\ g^{-1}$), suggesting that a relatively low SSA may contribute to the observed photocatalytic behavior.

The lower crystallinity and the presence of Fe- and Pb-containing impurities may also affect charge-carrier dynamics. Upon UV irradiation with photon energy equal to or greater than the ZnO band gap (~3.2 eV), electrons are excited from the valence band to the conduction band, generating electron–hole (e^-/h^+) pairs [38]. Structural defects can act as charge-trapping and recombination centers, thereby limiting charge migration to the catalyst surface and reducing the number of carriers available for photocatalytic reactions [39]. Fe and Pb impurities may additionally introduce electronic states within the ZnO band gap and modify charge-transfer kinetics. Although Fe^{3+} can act as a temporary charge trap and, under suitable conditions, suppress recombination, excessive Fe-related defect states may instead promote charge-carrier recombination. Pb-containing species may similarly introduce deep traps, form secondary oxide phases, or block surface-active sites, thereby adversely affecting photocatalytic activity [40,41]. Therefore, the combined effects of lower crystallinity, structural defects, and Fe- and Pb-containing impurities may contribute to enhanced charge-carrier recombination and less efficient interfacial charge transfer, providing an additional explanation for the almost zero photocatalytic activity observed for the hydrometallurgically produced ZnO.

Conversely, the pyrometallurgically produced ZnO exhibits a well-defined crystalline structure and finer morphology, which favors more efficient charge separation and provides a larger number of catalytically active surface sites, resulting in low photocatalytic performance (approximately 18% after 120 min. of irradiation).

The results obtained confirm that the method of preparation of ZnO fundamentally affects its microstructure and consequently its functional properties. While pyrometallurgical ZnO exhibits some photocatalytic effect in comparison to hydrometallurgical ZnO, both prepared samples visibly underperform commercial ZnO which degraded virtually all the Rhodamine B from the aqueous solution after just 60 min of irradiation. Hydro- and pyrometallurgically obtained ZnO are thus limited primarily by lower crystallinity and the presence of impurities, which limits their application potential without further purification or modification.

7. Conclusions

This study directly compared hydrometallurgical and pyrometallurgical routes for zinc recovery from mixed steelmaking and blast furnace sludge, with particular emphasis on how the recovery pathway affects the structural characteristics, purity, and functional properties of the resulting ZnO. The results confirmed that zinc mineralogy is a decisive factor governing both separation efficiency and final product quality.

Zinc in the investigated sludge occurred predominantly as chemically stable zinc ferrite (franklinite), which strongly limited its dissolution during acetic acid leaching. Consequently, the hydrometallurgical route resulted in only a 16.8% relative decrease in Zn content based on solid-phase concentrations and yielded ZnO containing elevated Fe- and Pb-bearing impurities. This product exhibited lower crystallinity, pronounced particle agglomeration, and negligible photocatalytic activity. In contrast, carbothermic treatment of the sludge–coke mixture at 1200 °C effectively decomposed zinc ferrite and promoted zinc volatilization, resulting in a 99.5% relative decrease in Zn content based on solid-phase concentrations and reducing the residual Zn content to below 0.05 wt.%. The pyrometallurgical route simultaneously generated highly crystalline wurtzite ZnO with low impurity levels and measurable photocatalytic activity toward RhB, together with an iron-rich residue potentially suitable for recycling into metallurgical processes.

The direct comparison further demonstrated that the characteristics of recovered ZnO are strongly determined by its formation mechanism. Solution-phase precipitation produced a less crystalline and more impurity-rich material, whereas gas-phase formation

during pyrometallurgical processing favoured higher crystallinity, improved purity, and enhanced functional performance.

A limitation of this study is that the experiments were performed on a single sludge composition under laboratory-scale conditions, while the functional evaluation of the recovered ZnO was limited to RhB photodegradation. Future work should therefore focus on process scale-up, evaluation of feedstock variability, optimization of energy and reagent consumption, and verification of the recovered ZnO and iron-rich residue in relevant industrial applications (for example rubber industry, friction composites).

Overall, the pyrometallurgical route provided a clear advantage for sludge in which zinc is predominantly bound in refractory ferritic phases. Beyond achieving nearly complete zinc separation, it enables simultaneous valorisation of both zinc and iron fractions, transforming a problematic metallurgical residue into potentially reusable secondary raw materials. These findings highlight the importance of considering zinc speciation and target product quality, rather than recovery efficiency alone, when selecting processing strategies for metallurgical wastes and support their integration into circular material flows within the iron and steel industry.

Author Contributions: Conceptualization, B.K. and V.M.; methodology, B.K., M.V. and V.M.; software, V.K.; validation, B.K., V.M. and M.V.; formal analysis, B.K., R.Š. and J.S.; investigation, B.K., R.Š., M.R., V.K., F.B., J.S. and S.V.; resources, J.V.; data curation, B.K.; writing—original draft preparation, B.K., R.Š.,V.M. and M.V.; writing—review and editing, B.K., V.M., M.V. and R.Š.; visualization, B.K., F.B., R.Š. and V.M.; supervision, B.K.; project administration, J.V.; funding acquisition, J.V. All authors have read and agreed to the published version of the manuscript.

Funding: This work was supported by the European Just Transition Fund within the Operational Programme Just Transition under the Ministry of the Environment of the Czech Republic, project CirkArena (CZ.10.03.01/00/22_003/0000045).

Institutional Review Board Statement: Not applicable.

Informed Consent Statement: Not applicable.

Data Availability Statement: The raw data supporting the conclusions of this article will be made available by the authors on request.

Acknowledgments: This work was supported by the European Just Transition Fund within the Operational Programme Just Transition under the Ministry of the Environment of the Czech Republic, project CirkArena (CZ.10.03.01/00/22_003/0000045) and by the Ministry of the Environment of the Czech Republic, Vouchers for universities in the Moravian-Silesian Region–1st Call [CZ.10.03.01/00/23_042/0000390].

Conflicts of Interest: Bruno Kostura, Vladislav Kůrka and Jozef Vlček were employed by The Material and Metallurgical Research, Co., Ltd. The remaining authors declare that the research was conducted in the absence of any commercial or financial relationships that could be construed as a potential conflict of interest.

References

1. Das, B.; Prakash, S.; Reddy, P.S.R.; Misra, V.N. An overview of utilization of slag and sludge from steel industries. *Resour. Conserv. Recycl.* **2007**, *50*, 40–57. [CrossRef]
2. Havlík, T.; Turzáková, M.; Stopić, S.; Friedrich, B. Atmospheric leaching of EAF dust with diluted sulphuric acid. *Hydrometallurgy* **2005**, *77*, 41–50. [CrossRef]
3. Li, Y.-C.; Zhuo, S.-N.; Peng, B.; Min, X.-B.; Liu, H.; Ke, Y. Comprehensive recycling of zinc and iron from smelting waste containing zinc ferrite by oriented transformation with SO_2. *J. Clean. Prod.* **2020**, *263*, 121468. [CrossRef]
4. Oustadakis, P.; Tsakiridis, P.E.; Katsiapi, A.; Agatzini-Leonardou, S. Hydrometallurgical process for zinc recovery from electric arc furnace dust (EAFD). Part I. *J. Hazard. Mater.* **2010**, *179*, 1–7. [CrossRef]

5. European Commission. Best Available Techniques (BAT) conclusions for Iron and Steel Production. *Off. J. Eur. Union* **2012**, *70*, 63–98.
6. Hosseini, A.; Moosavi-Khoonsari, E.; Meijer, K.; Hage, J.; Peeters, T.; Offerman, E.; Yang, Y. Thermodynamic analysis of zinc ferrite ($ZnFe_2O_4$) formation inside the HIsarna off-gas system. *Ironmak. Steelmak. Process. Prod. Appl.* **2023**, *50*, 485–499. [CrossRef]
7. Andersson, A.; Gullberg, A.; Kullerstedt, A.; Ahmed, H.; Sundqvist-Ökvist, L.; Samuelsson, C. Upgrading of Blast Furnace Sludge and Recycling of the Low-Zinc Fraction via Cold-bonded Briquettes. *J. Sustain. Metall.* **2019**, *5*, 350–361. [CrossRef]
8. Binnemans, K.; Jones, P.T.; Fernández, A.M.; Torres, V.M. Hydrometallurgical Processes for the Recovery of Metals from Steel Industry By-Products: A Critical Review. *J. Sustain. Metall.* **2020**, *6*, 505–540. [CrossRef]
9. Duan, W.; Dong, X.; Gao, L.; Wang, Z.; Wang, J. Zn recovery strategies from steelmaking dust: A comprehensive review. *Sep. Purif. Technol.* **2025**, *378*, 134694. [CrossRef]
10. Antuñano, N.; Cambra, J.F.; Arias, P.L. Hydrometallurgical processes for Waelz oxide valorisation—An overview. *Process Saf. Environ. Prot.* **2019**, *129*, 308–320. [CrossRef]
11. Wang, Y.; Liu, B.; Sun, H.; Huang, Y.; Han, G. Selective extraction and recovery of tin from hazardous zinc-leaching residue by oxalic acid/sulfuric acid mixture leaching and hydrolytic precipitation. *J. Clean. Prod.* **2022**, *342*, 130955. [CrossRef]
12. Bao, S.; Chen, B.; Zhang, Y.; Ren, L.; Xin, C.; Ding, W.; Yang, S.; Zhang, W. A comprehensive review on the ultrasound-enhanced leaching recovery of valuable metals: Applications, mechanisms and prospects. *Ultrason. Sonochem.* **2023**, *98*, 106525. [CrossRef]
13. Hamann, C.; Piehl, P.; Weingart, E.; Stolle, D.; Al-Sabbagh, D.; Ostermann, M.; Auer, G.; Adam, C. Selective removal of zinc and lead from electric arc furnace dust by chlorination–evaporation reactions. *J. Hazard. Mater.* **2024**, *465*, 133421. [CrossRef]
14. Kaya, M.; Hussaini, S.; Kursunoglu, S. Critical review on secondary zinc resources and their recycling technologies. *Hydrometallurgy* **2020**, *195*, 105362. [CrossRef]
15. Langová, Š.; Kostura, B.; Raška, P.; Matýsek, D.; Novák, V.; Ritz, M.; Krčmář, J. Electrochemical characterization of leached steel-making sludge. *Sci. Rep.* **2022**, *12*, 16691. [CrossRef]
16. Wang, J.; Wang, Z.; Zhang, Z.; Zhang, G. Removal of zinc from basic oxygen steelmaking filter cake by selective leaching with butyric acid. *J. Clean. Prod.* **2019**, *209*, 1–9. [CrossRef]
17. Steer, J.M.; Griffiths, A.J. Investigation of carboxylic acids and non-aqueous solvents for the selective leaching of zinc from blast furnace dust slurry. *Hydrometallurgy* **2013**, *140*, 34–41. [CrossRef]
18. Zheng, X.; Li, X.; Wang, X. A Study on the Mechanism and Kinetics of Ultrasound-Enhanced Sulfuric Acid Leaching for Zinc Extraction from Zinc Oxide Dust. *Materials* **2022**, *15*, 5969. [CrossRef]
19. Xin, C.; Bao, S.; Zhang, Y.; Chen, B.; Ding, W.; Gan, W. Selective leaching mechanisms of zinc from industrial waste using hybrid acids: Sustainable synthesis of nano-ZnO. *J. Environ. Manag.* **2025**, *373*, 123528. [CrossRef]
20. Wang, S.; Xu, C.; Lei, Z.; Li, J.; Lu, J.; Xiang, Q.; Chen, X.; Hua, Y.; Li, Y. Recycling of zinc oxide dust using ChCl-urea deep eutectic solvent with nitrilotriacetic acid as complexing agents. *Miner. Eng.* **2021**, *175*, 107295. [CrossRef]
21. Radzymińska-Lenarcik, E.; Sulewski, M.; Urbaniak, W. Recovery of Zinc from Metallurgic Waste Sludges. *Pol. J. Environ. Stud.* **2015**, *24*, 1277–1282. [CrossRef]
22. Wang, J.; Zhang, Y.; Cui, K.; Fu, T.; Gao, J.; Hussain, S.; AlGarni, T.S. Pyrometallurgical recovery of zinc and valuable metals from electric arc furnace dust—A review. *J. Clean. Prod.* **2021**, *298*, 126788. [CrossRef]
23. Vogelbacher, M.; Keller, S.; Zehm, W.; Matthes, J. Advanced Methods for Kiln-Shell Monitoring to Optimize the Waelz Process for Zinc Recycling. *Processes* **2021**, *9*, 1062. [CrossRef]
24. Grudinsky, P.; Yurtaeva, A.; Pankratov, D.; Pasechnik, L.; Musaelyan, R.; Dyubanov, V. The Waelz Slag from Electric Arc Furnace Dust Processing: Characterization and Magnetic Separation Studies. *Materials* **2024**, *17*, 2224. [CrossRef]
25. Simoni, M.; Reiter, W.; Suer, J.; Di Sante, L.; Cirilli, F.; Praolini, F.; Mosconi, M.; Guzzon, M.; Malfa, E.; Algermissen, D.; et al. Towards the Circularity of the EU Steel Industry: Modern Technologies for the Recycling of the Dusts and Recovery of Resources. *Metals* **2024**, *14*, 233. [CrossRef]
26. Qin, X.; Xu, H.; Zhang, G.; Wang, J.; Wang, Z.; Zhao, Y.; Wang, Z.; Tan, T.; Bockstaller, M.R.; Zhang, L.; et al. Enhancing the Performance of Rubber with Nano ZnO as Activators. *ACS Appl. Mater. Interfaces* **2020**, *12*, 48007–48015. [CrossRef]
27. Alam, M.N.; Kumar, V.; Park, S.S. Advances in Rubber Compounds Using ZnO and MgO as Co-Cure Activators. *Polymers* **2022**, *14*, 5289. [CrossRef]
28. Škuta, R.; Kostura, B.; Langová, Š.; Ritz, M.; Foniok, K.; Študentová, S.; Pavlovský, J.; Novák, V.; Matýsek, D. Utilization of metallurgical waste for the preparation of photocatalytically active composites based on ZnO–graphene oxide. *Chem. Pap.* **2021**, *75*, 3891–3900. [CrossRef]
29. Wei, J.; Pei, Q.; Xia, H.; Xu, Y.; Dai, L.; Zhang, L. Unlocking zinc ferrite via DFT-revealed mechanisms: Synergistic ultrasound-tartaric acid leaching for critical metal recovery. *J. Environ. Chem. Eng.* **2025**, *13*, 118700. [CrossRef]
30. Rakhmataliev, S.A.U.; Khojiev, S.T.; Turan, M.D.; Kholikulov, D.B.; Khaydaraliev, K.R.U. Hydrazine-Assisted Reductive Leaching of Zinc Cake: Thermodynamic Assessment, RSM Optimization, and Microstructural Evolution of Refractory Residues. *J. Sustain. Metal.* **2026**. [CrossRef]

31. Zhu, T.; Feng, S.; Cao, J.; Wang, W.; Li, M.; Wang, X.; Sun, Y. Calcium-Enhanced Reduction Mechanism of Iron-Rich Zinc-Bearing Spinel. *Metall. Mater. Trans. B* **2026**, *57*, 5493–5505. [CrossRef]
32. Mousa, M.A.; Gomaa, E.A.; Khairy, M.; Eltanany, M.E. Thermodynamic and Thermal Properties of Solvation for Nano Nickel Ferrite and Nano Zinc Ferrite Prepared by the Sol–Gel Method in Different CH_3COOH Concentrations at Different Temperatures. *J. Inorg. Organomet. Polym. Mater.* **2020**, *30*, 417–426. [CrossRef]
33. Ziezio, M.; Charmas, B.; Jedynak, K.; Hawryluk, M.; Kucio, K. Preparation and characterization of activated carbons obtained from the waste materials impregnated with phosphoric acid(V). *Appl. Nanosci.* **2020**, *10*, 4703–4716. [CrossRef]
34. Li, X.; Guo, L.-J.; Li, W.-C. Experimental Study on Physical Excitation of Cementitious Activity of Lead-zinc Smelting Slag. *IOP Conf. Ser. Earth Environ. Sci.* **2020**, *525*, 012154. [CrossRef]
35. Niu, X.; Li, M.; Wang, H.; Ma, L.; Wang, S.; Zhou, T.; Wang, W. Historical Lead Smelting Slag Harmlessness and Valuable Metals Recovery: A Co-Treatment of Lead Slag and Zinc-Bearing Material in Rotary Kiln. *Sustainability* **2022**, *14*, 13647. [CrossRef]
36. Li, X.B.; Zhang, Q.Q.; Ma, S.Y.; Wan, G.X.; Li, F.M.; Xu, X.L. Microstructure optimization and gas sensing improvement of ZnO spherical structure through yttrium doping. *Sens. Actuators B Chem.* **2014**, *195*, 526–533. [CrossRef]
37. Zhang, Y.; Ma, Z.; Gu, X.; Jia, S.; An, X.; Niu, M.; Zha, X.; He, R.; Deng, R. A review of metallurgical processing and value-added utilization strategies for zinc oxide. *Sci. Prog.* **2026**, *109*, 1–15. [CrossRef]
38. Zhu, C.; Wang, X. Nanomaterial ZnO Synthesis and Its Photocatalytic Applications: A Review. *Nanomaterials* **2025**, *15*, 682. [CrossRef]
39. Chen, D.; Wang, Z.; Ren, T.; Ding, H.; Yao, W.; Zong, R.; Zhu, Y. Influence of Defects on the Photocatalytic Activity of ZnO. *J. Phys. Chem. C* **2014**, *118*, 15300–15307. [CrossRef]
40. Dao, D.V.; van den Bremt, M.; Koeller, Z.; Le, T.K. Effect of metal ion doping on the optical properties and the deactivation of photocatalytic activity of ZnO nanopowder for application in sunscreens. *Powder Technol.* **2016**, *288*, 366–370. [CrossRef]
41. Bouri, A.; Bessadok, M.N.; Bouzidi, C.; Alyamani, A.; El Mir, L. Development of a Pb-doped ZnO nanoparticles-based sensor for luminescence thermometry applications. *J. Lumin.* **2026**, *293*, 121809. [CrossRef]

Disclaimer/Publisher's Note: The statements, opinions and data contained in all publications are solely those of the individual author(s) and contributor(s) and not of MDPI and/or the editor(s). MDPI and/or the editor(s) disclaim responsibility for any injury to people or property resulting from any ideas, methods, instructions or products referred to in the content.